Dynamical amplification of polar warming

Ming Cai

Department of Meteorology, Florida State University, Tallahassee, Florida, USA

Received 25 August 2005; revised 10 October 2005; accepted 18 October 2005; published 29 November 2005.

[1] This paper presents theoretical and modeling evidence suggesting that the atmospheric poleward heat transport can lead to a polar warming amplification (i) by redistributing part of the extra energy intercepted by the low-latitude atmosphere to high latitudes, and (ii) by strengthening the water vapor feedback in high latitudes. For an anthropogenic radiative forcing of 4 Wm^{-2}, we illustrate that the dynamical amplifier contributes to about 1/4 (1/10) of the total high-latitude (global) surface warming in winter in a simple coupled atmosphere-surface moist radiative-transportive climate model. Budget analysis of the radiation fluxes at the top of the atmosphere derived from IPCC AR4 CGCM climate simulations seems to support the dynamical amplifier theory for the larger warming in high latitudes.
Citation: Cai, M. (2005), Dynamical amplification of polar warming, *Geophys. Res. Lett.*, *32*, L22710, doi:10.1029/2005GL024481.

1. Introduction

[2] The recent Arctic Climate Impact Assessment reports that "annual average Arctic temperature has increased at almost twice the rate as the rest of the world over the past few decades" [*Hassol*, 2004]. Furthermore, the rapid surface warming in high-latitudes is particularly pronounced in winter [*Houghton et al.*, 2001; *Hansen et al.*, 1999; *Jones et al.*, 1999]. Local thermodynamic feedbacks can contribute to a relatively larger surface warming in high latitudes through the ice-albedo feedback that amplifies the high latitude warming [*Manabe*, 1983; *Hall*, 2004] and through the evaporation feedback that more strongly damps the low latitude surface warming [*Hassol*, 2004]. The global surface warming is also amplified by the water vapor feedback [*Manabe and Wetherald*, 1967; *Cess*, 1989; *Hartmann*, 1994; *Hall and Manabe*, 1999, 2000].

[3] We use a 4-box coupled atmosphere-surface moist radiative-transportive climate model to illustrate the dynamical amplification of the high-latitude surface warming due to an anthropogenic forcing. Listed in Tables 1–4 are the model variables, equations, constants, parameters and their values, respectively. Two of the 4 boxes represent the low-latitude atmosphere column and the surface box below (variables with subscript j = 1) and the other two the high-latitude atmosphere and surface (variables with subscript j = 2). All boxes have an equal area, representing one half of the total hemispheric surface area. In addition to surface and atmosphere temperatures, the model includes variables associated with water cycle, namely, specific humidity, evaporation, and precipitation for both low- and high-latitude boxes. As a result, both poleward sensible and latent heat transport has been taken into consideration. Equations 1 and 2 listed in Table 2 are the energy balance equations for the surface and atmosphere boxes, respectively. The remaining three equations are the parameterizations for evaporation, ice-albedo, and water vapor feedbacks. Because of the lack of detailed atmospheric dynamics and physics, cloud feedback is not included in this simple model. The ice-albedo feedback is parameterized as in Equation 4 listed in Table 2, which has been commonly used in a simple energy balance model [*Budyko*, 1969; *Sellers*, 1969; *North*, 1975]. The water vapor feedback has been crudely parameterized using an ad-hoc formula Equation 5 to mimic the strong dependency of the atmospheric absorption of longwave radiation to the amount of water vapor. Specifically, the total atmospheric effective emissivity in the model is made of two parts: a constant part ε_0 representing the absorption due to other gases, such as CO_2, and a part that varies as a function of the total amount of water vapor in an atmosphere column. A smaller (larger) value of ε_0 indirectly implies a stronger (weaker) water vapor feedback relative to the ice-albedo feedback. Other than this, the results are not sensitive to ε_0. In order to ensure the total amount of water vapor within each of the two atmosphere columns is realistic, which directly affects the model's atmospheric effective emissivity, we use $\overline{T}_j = 0.6G_j + 0.4A_j$ for evaluating the saturated water vapor in the two air columns. For a water vapor amount varying from 44 to 3.2 kg/m^2, the ad hoc formula Equation 5 yields total atmospheric effective emissivity ranging from 0.92 in the low-latitude atmosphere column to 0.78 in the high-latitude air column, implying that only about 10–20% surface terrestrial radiation would escape to space as in nature. In a steady equilibrium state, the atmosphere is saturated and evaporation and precipitation rates are constant in time. The latent heat associated with condensation, which is exactly equal to precipitation in an equilibrium state, is included in Equation (2). The global warming scenario is modeled by adding a perturbation $\Delta\varepsilon = 0.03$ to the base emissivity in each of the two air columns, corresponding to about a global mean radiative forcing of 4 Wm^{-2} (referred to as the $2 \times CO_2$ forcing). Because the strong dependency of saturated water vapor on temperature, the total change in emissivity varies with latitude and is larger than the original perturbation of $\Delta\varepsilon = 0.03$.

2. Results

[4] To gain a better understanding of the dynamical amplifier, let us first discuss the analytical solution of this model obtained in a dry model setting in which sensible and latent surface fluxes, water vapor and ice-albedo feedbacks and poleward latent heat transport are all absent (i.e., $\nu_L = \nu_S = 0$, $\varepsilon_1 = \varepsilon_2 = \varepsilon$ = constant, α_1 and α_2 are constants, $\mu_q = 0$).

0094-8276/05/2005GL024481

Table 1. List of Variables and the Solution at $\mu_T = 3\ \mathrm{Wm^{-2}K^{-1}}$, $\mu_q = 0.24\ \mathrm{Wm^{-2}kg^{-1}}$ [a]

Surface Temperature	Atmosphere Temperature	Specific Humidity	Evaporation Rate	Precipitation Rate	Effective Emissivity	Surface Albedo
G_j(K)	A_j (K)	q_j	E_j (kg $\mathrm{s^{-1}m^{-2}}$)	P_j (kg $\mathrm{s^{-1}m^{-2}}$)	ε_j	α_j
$G_1 = 292.4$ K	$A_1 = 249.1$ K	$m_a q_1 = 44$ kg/m^2	$E_1 = 2.01$ kg/d/m^2	$P_1 = 1.67$ kg/d/m^2	$\varepsilon_1 = 0.92$	$\alpha_1 = 0.2$
$G_2 = 250.6$ K	$A_2 = 231.2$ K	$m_a q_2 = 3.2$ kg/m^2	$E_2 = 0.07$ kg/d/m^2	$P_2 = 0.40$ kg/d/m^2	$\varepsilon_2 = 0.78$	$\alpha_2 = 0.28$

[a]The solutions for the low latitude and high latitude variables are given in the 3rd and 4th rows, respectively and $P_j = E_J + (-1)^j\, \mu_q m_A\, [q_1 - q_2]/L$.

The change in the equator-to-pole air temperature contrast forced by $\Delta\varepsilon \neq 0$ is

$$\Delta(A_1 - A_2) = \frac{\sigma A_{E1}^3 A_{E2}^3 + \mu_T \dfrac{A_{E1}^3 + A_{E2}^3}{\varepsilon^2}}{4\sigma A_{E1}^3 A_{E2}^3 + \mu_T \dfrac{A_{E1}^3 + A_{E2}^3}{(2-\varepsilon)\varepsilon}} (A_{E1} - A_{E2}) \frac{\Delta\varepsilon}{2-\varepsilon} \quad (1)$$

where the subscript "E" denotes the equilibrium solution satisfying the dry model version of the model equations in the absence of the forcing ($\Delta\varepsilon = 0$). The change in surface temperature is

$$\Delta G_j = \frac{G_{Ej}}{4} \frac{\Delta\varepsilon}{(2-\varepsilon)} + (-1)^j \mu_T \frac{\Delta(A_1 - A_2)}{4\sigma G_{Ej}^3 (2-\varepsilon)} \quad (2)$$

It follows that a positive $\Delta\varepsilon$ always leads to an increase in the atmospheric equator-to-pole temperature contrast since $A_{E1} > A_{E2}$. It is seen from (2) that the strengthening of the atmospheric equator-to-pole temperature contrast implies a positive (negative) feedback on the surface temperature warming in high (low) latitudes. From a physics point of view, the extra amount of energy intercepted by the low-latitude atmosphere due to its higher opacity is partially transported to high latitudes by the strengthened atmospheric poleward heat transport. Therefore, only part of the extra amount of radiation energy intercepted by the low-latitude atmosphere is available to warm the surface below. This dynamically induced "greenhouse-minus" feedback reduces the surface warming in low latitudes. Conversely, the extra amount of heat transported to high latitudes acts as an additional energy source to the high-latitude air mass. As a result, the high-latitude air mass has to emit more radiation energy to the space and to the surface below than the extra amount of radiation energy it intercepts from the surface due to an increase in its opacity. This dynamically induced "greenhouse-plus" feedback causes additional surface warming in high latitudes. As to be shown shortly, the net effect of the second term in (2), namely the additional high latitude surface warming plus the reduction of the low latitude surface warming, can exceed the first term, resulting in a stronger surface warming in high latitudes than in low latitudes. Because of the Stefan-Boltzmann feedback [*Hartmann*, 1994], namely the factor G_{Ej}^3 in the denominator of (2), the negative dynamical feedback in low-latitudes is suppressed more strongly than the positive one in high latitudes. It follows that the negative dynamical feedback in low latitudes cannot cancel out the positive dynamical feedback in high latitudes, leading to a further increase of the global mean surface temperature from the warming due to the radiative forcing alone.

[5] We next wish to explore how the dynamical feedbacks further amplify the enhanced surface warming due to local thermodynamical feedbacks in response to an anthropogenic forcing. The numerical solutions are obtained by varying μ_T from 0 to 10 $\mathrm{Wm^{-2}}$ with winter solar forcing S_j listed in Table 4. Different values of μ_T can be regarded to correspond to different models that have a different strength of the poleward heat transport for a winter hemisphere. Particularly, $\mu_T = 0$ corresponds to a model that does not include the poleward heat transport. A larger value of μ_T yields a stronger poleward heat transport and gives rise to an

Table 2. List of Model Equations

	Equation
Equation 1	$\sigma G_j^4 - \varepsilon_j \sigma A_j^4 = (1-\alpha_j) S_j - L E_j - \upsilon_S (G_j - A_j)$
Equation 2	$2\varepsilon_j \sigma A_j^4 - \varepsilon_j \sigma G_j^4 = \upsilon_S (G_j - A_j) + L E_j + (-1)^j \left\{ \mu_q m_A \left[q_s(\overline{T}_1) - q_s(\overline{T}_2) \right] + \mu_T (A_1 - A_2) \right\}$
Equation 3	$E_j = \frac{\upsilon_L}{L} m_A \left[q_s(G_j) - q_s(\overline{T}_j) \right]$, where $\overline{T}_j = 0.6 G_j + 0.4 A_j$
Equation 4	$\alpha_j = \begin{cases} 0.2 & G_j \geq 270\mathrm{K} \\ 0.2 + 0.4 \dfrac{270 - G_2}{100} & 170\mathrm{K} < G_j < 270\mathrm{K} \\ 0.6 & G_j \leq 170\mathrm{K}. \end{cases}$
Equation 5	$\varepsilon_j = \varepsilon_0 + (1-\varepsilon_0) \tanh^{1/4} \left(\dfrac{m_A q_s(\overline{T}_j)}{100} \right) + \Delta\varepsilon$, where $q_s(T) = 0.622 \dfrac{6.11}{1000} e^{\frac{L}{R_V}\left(\frac{1}{273.15} - \frac{1}{T}\right)}$

Table 3. List of Model Parameters and Their Standard Settings

Parameter	Setting
Sensible heat transport coefficient, $Wm^{-2}K^{-1}$	μ_T: 0–10
Latent heat transport coefficient, $Wm^{-2}kg^{-1}$	$\mu_q = 0.08\ \mu_T$
Surface sensible heat flux coefficient, $Wm^{-2}K^{-1}$	$\upsilon_S = 0.6$
Surface latent heat flux coefficient, $Wm^{-2}kg^{-1}$	$\upsilon_L = 0.6$
Effective emissivity due to gases other than H_2O	$\varepsilon_0 = 0.6$

equilibrium solution that is further from the radiative equilibrium solution. We will examine the dependency of the thermodynamic feedbacks and dynamical amplifier on the strength of the poleward heat transport. The results presented in this paper are not sensitive to the choices of numerical values of the model parameters listed in Table 3 as far as the dynamical amplification is concerned.

[6] We first obtain the solution of Equations 1–5 listed in Table 2 with $\Delta\varepsilon = 0.0$, which is referred to as the **1CO2** solution (the **1CO2** solution with $\mu_T = 3\ Wm^{-2}K^{-1}$ is listed in Table 1 and the corresponding poleward (sensible and latent) heat transport from the low- to high-latitude atmosphere box is about 8.1 PW). We then obtain the equilibrium solutions with $\Delta\varepsilon = 0.03$ for the following 4 experiments:

[7] i) **2CO2_TD** (red curves in Figure 1): As in **1CO2** except $\Delta\varepsilon = 0.03$.

[8] ii) **2CO2_00** (black curves in Figure 1): Same as in **2CO2_TD** except that all terms on the RHS of Equations 1 and 2 are held at the same values as **1CO2**.

[9] iii) **2CO2_0D** (green curves in Figure 1): Same as **2CO2_00** except that the terms inside the bracket "{}" in Equation 2 are allowed to change accordingly.

[10] iv) **2CO2_T0** (blue curves in Figure 1): Same as **2CO2_TD** except that the terms inside the bracket "{}" in Equation 2 are held at the same values as **1CO2**.

[11] The differences of **2CO2_00**, **2CO2_0D**, **2CO2_T0** from **1CO2**, respectively, are the warmings due to the $2 \times CO_2$ forcing only, the $2 \times CO_2$ forcing plus only the dynamical feedback due to the poleward transport of both sensible and latent heat, and the $2 \times CO_2$ forcing plus only the local thermodynamic feedbacks. The difference between **2CO2_TD** and **1CO2** is the total warming due to the $2 \times CO_2$ forcing plus both local thermodynamic and non-local dynamical feedbacks.

[12] Figure 1 shows the surface temperature change derived from these four global warming experiments as a function of the strength of the poleward heat transport of the **1CO2** solution (the abscissa). The most important feature of the **2CO2_00** solution (the black curves) is that in the absence of any feedbacks, the surface warming due to the $2 \times CO_2$ forcing alone is always stronger in low latitudes. The dynamical feedback alone (**2CO2_0D**: green curves) acts to amplify (damp) the high (low) latitude surface warming due to the greenhouse-plus (greenhouse-minus) feedback to the high (low) latitude surface warming. This can lead to a larger surface warming in high latitudes in a model that has a sufficiently strong poleward heat transport (e.g., greater than 7 PW or $\mu_T > 2.1\ Wm^{-2}K^{-1}$) in the mean state. Such a polar amplification of global warming without ice-albedo feedback has been demonstrated in GCM simulations [*Hall*, 2004; *Schneider et al.*, 1997; *Alexeev et al.*, 2005]. As shown in (2), the Stefan-Boltzmann feedback suppresses the greenhouse-minus dynamical feedback in low latitudes more strongly than the greenhouse-plus feedback in high latitudes. As a result, the dynamical amplifier also strengthens the global surface warming (green vs. black curves in the bottom panel of Figure 1). We have also carried out an experiment similar to 2CO2_0D except that only the dynamical feedback due to sensible heat transport is considered as in the analytical dry model solution (2). As expected, the dynamical amplification only due to sensible heat transport is smaller and the gradient of the surface temperature warming is reversed at $\mu_T = 3.2\ Wm^{-2}K^{-1}$ instead of $\mu_T = 2.1\ Wm^{-2}K^{-1}$.

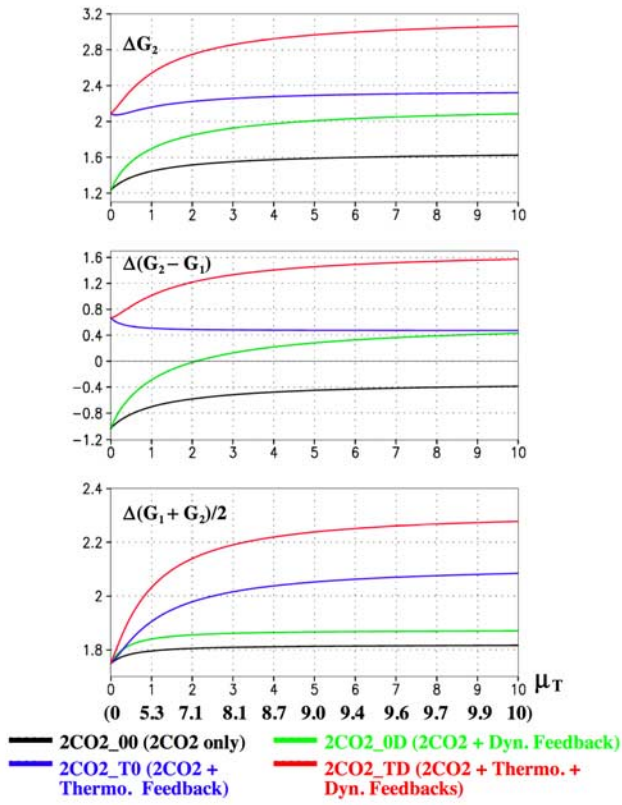

Figure 1. Perturbation solution forced by a "$2 \times CO_2$ forcing" (a change in the atmospheric effective emissivity $\Delta\varepsilon = 0.03$) for winter season solar forcing. Top panel: High-latitude surface temperature change; Middle panel: Difference between high- and low-latitude surface temperature changes; Bottom panel: Global mean surface temperature change. The unit of ordinate is K. The unit of $\boldsymbol{\mu_T}$ (abscissa) is $Wm^{-2}K^{-1}$. The numbers in the parenthesis below the abscissa label are the corresponding (sensible and latent) heat transport from the low- to high-latitude atmosphere box (unit: PW) in the unperturbed climate state for a winter hemisphere.

Table 4. List of Model Constants

Constant	Value
S_1	$372\ Wm^{-2}$
S_2	$156\ Wm^{-2}$
σ	$5.67 \times 10^{-8}\ Wm^{-2}K^{-4}$
m_A	$10^4\ kg\ m^{-2}$
L	$2.5 \times 10^6\ J\ kg^{-1}$
R_v	$461\ JK^{-1}kg^{-1}$

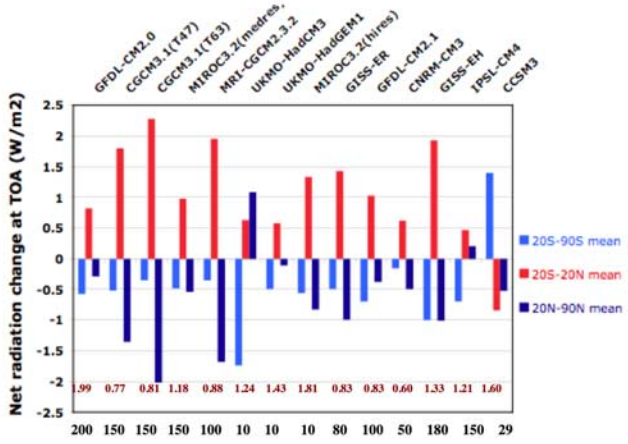

Figure 2. Areal average difference of the long-time averaged net radiation flux at the TOA between the control (IPCC AR4 EXP1) and the 2 × CO_2 experiments (IPCC AR4 EXP8) derived from 14 IPCC AR4 model simulations (http://www-pcmdi.llnl.gov/ipcc/about_ipcc.php). The official model names are indicated above the bars. The global mean value (in unit of W/m^2) of each model, which is indicated below the bars (brown-font numbers), has been taken out before the areal mean is calculated. The numbers of the x-axis label are the years for the time averaging, which equals to all available years after the IPCC AR4 EXP8 experiment reaches to the 2 × CO_2 level for each model.

[13] The blue curves in Figure 1 represent the warming due to the 2CO2 forcing plus the thermodynamical feedbacks (**2CO2_T0**). It is seen that the surface warming in both low and high latitudes is stronger when the mean poleward heat transport is stronger. This implies that the strength of thermodynamic feedbacks depends not only on the external radiative forcing, but also strongly on the strength of the poleward heat transport in the mean state. However, the extra high-latitude surface warming with respect to the low-latitude in the experiment 2CO2_T0, which is primarily due to the ice-albedo, varies little with the strength of the mean poleward heat transport.

[14] The red curves in Figure 1 are the total surface warming derived from the difference between the **2CO2_TD** and **1CO2** solutions. It is seen that the dynamical amplification of the high latitude surface warming is more pronounced in **2CO2_TD** than in **2CO2_0D** (e.g., the gap between the red and blue curves is wider than the gap between the green and black curves). The further diagnosis suggests that because of the ice-albedo feedback, the change in the poleward heat transport in **2CO2_TD** actually is slightly smaller than that in **2CO2_0D** (not shown). It turns out that dynamical feedbacks also indirectly act to strengthen (reduce) the water vapor feedback in high (low) latitudes by increasing (reducing) water vapor presence in high (low) latitudes. In this sense, the dynamical feedback amplifies the signal not only through an enhanced poleward heat transport but also by strengthening the water vapor feedback in high latitudes. For μ_T = 3 $Wm^{-2}K^{-1}$, corresponding to a poleward (sensible and latent) heat transport of 8.1 PW from the low to high latitudes in winter season, the dynamical amplifier in this simple model contributes to 0.60 K to the total surface warming of 2.86 K in high latitudes. It also adds a 0.17 K warming to the total global surface warming of 2.19 K.

3. Modeling Evidence

[15] The dynamical amplifier mechanism requires a net increase of poleward heat transport in response to an anthropogenic radiative forcing. Such an enhanced poleward heat transport must imply an increase in net radiation energy surplus (deficit) in low- (high-) latitudes. Because the dynamical amplifier is automatically built in a coupled general circulation model, one can deduce the high-latitude surface warming due to the dynamical amplifier feedback in a general circulation climate model from the change of deficit (surplus) of the net radiation flux at the top of the atmosphere (TOA). It should be emphasized here that after the system reaches a new equilibrium state, one would not be able to identify such a change in the net radiation flux at the TOA if the amplified warming in high latitudes were caused purely by local thermodynamic feedbacks.

[16] Plotted in Figure 2 are differences of the net radiation energy flux at the TOA between the 2 × CO_2 and the standard climate simulations derived from14 IPCC AR4 CGCM climate simulation outputs. It is seen that the majority (11 out of 14) of climate model simulations clearly show an intensification of net radiation energy surplus (deficit) in low (high) latitudes at the TOA, as suggested by the dynamical amplifier theory. It is known that a change in the radiative energy flux imbalance at the TOA may also reflect a change in the oceanic heat transport or ocean heat storage. We have also calculated the atmospheric heat transport inferred from both the TOA and surface energy fluxes of IPCC AR4 climate simulations. All 8 IPCC AR4 simulations we analyzed show a stronger atmospheric poleward heat transport in the 2 × CO_2 simulations, including the UKMO-HadCM3 simulations (this implies that the 2 × CO_2 simulation by the UKMO-HadCM3 model has a substantial reduction in the oceanic poleward heat).

4. Summary

[17] In this paper, we report analytical and numerical solutions of a 4-box coupled atmosphere-surface moist radiative-transportive climate model in an attempt to illustrate the dynamical amplification mechanism of the high-latitude surface warming due to an anthropogenic forcing. For an anthropogenic radiative forcing of 4 Wm^{-2}, we found that the dynamical feedback in this simple model contributes to about 1/4 (1/10) of the total high-latitude (global) surface warming in winter. Budget analysis of the radiation fluxes at the top of the atmosphere derived from IPCC AR4 CGCM climate simulations is consistent with the dynamical amplifier theory for the larger warming in high latitudes.

[18] **Acknowledgments.** The author acknowledges the international modeling groups for providing their data for analysis, the Program for Climate Model Diagnosis and Intercomparison (PCMDI) for collecting and archiving the model data, the JSC/CLIVAR Working Group on Coupled Modelling (WGCM) and their Coupled Model Intercomparison Project (CMIP) and Climate Simulation Panel for organizing the model data analysis activity, and the IPCC WG1 TSU for technical support. The IPCC

Data Archive at Lawrence Livermore National Laboratory is supported by the Office of Science, U.S. Department of Energy. The author wishes to thank Minfeng Zhang for his assistance in running the models and Christell Castet for analyzing the IPCC AR4 model outputs. The suggestions on the first draft of this paper from Bob Hart are greatly appreciated. The author is grateful to the two anonymous reviewers for their helpful suggestions. This work was supported by an NSF grant ATM ATM-0403211.

References

Alexeev, V. A., P. L. Langen, and J. R. Bates (2005), Polar amplification of surface warming on an aquaplanet in "ghost forcing" experiments without sea ice feedbacks, *Clim. Dyn.*, *24*, 655–666.

Budyko, M. J. (1969), The effect of solar radiation variation on the climate of the Earth, *Tellus*, *21*, 611–619.

Cess, R. D. (1989), Gauging water-vapor feedback, *Nature*, *342*, 736–737.

Hall, A. (2004), The role of surface albedo feedback in climate, *J. Clim.*, *17*, 1550–1568.

Hall, A., and S. Manabe (1999), The role of water vapor feedback in unperturbed climate variability and global warming, *J. Clim.*, *12*, 2327–2346.

Hall, A., and S. Manabe (2000), Effect of water vapor feedback on internal and anthropogenic variations of the global hydrologic cycle, *J. Geophys. Res.*, *105*, 6935–6944.

Hansen, J., R. Ruedy, J. Glascoe, and M. Sato (1999), GISS analysis of surface temperature change, *J. Geophys. Res.*, *104*, 30,997–31,022.

Hartmann, D. L. (1994), *Global Physical Climatology*, pp. 231–245, Elsevier, New York.

Hassol, S. J. (2004), *Impacts of a Warming Arctic: Arctic Climate Impact Assessment*, 146 pp., Cambridge Univ. Press, New York.

Houghton, J. T., et al. (2001), *Climate Change 2001: The Scientific Basis*, pp. 101–181, Cambridge Univ. Press, New York.

Jones, P. D., M. New, D. E. Parker, S. Martin, and I. G. Rigor (1999), Surface air temperature and its changes over the past 150 years, *Rev. Geophys.*, *37*, 137–199.

Manabe, S. (1983), Carbon dioxide and climate change, *Adv. Geophys.*, *25*, 39–80.

Manabe, S., and R. T. Wetherald (1967), Thermal equilibrium of the atmosphere with a given distribution of relative humidity, *J. Atmos. Sci.*, *24*, 241–259.

North, G. R. (1975), Theory of energy-balance climate models, *J. Atmos. Sci.*, *32*, 2033–2043.

Schneider, E. K., R. L. Lindzen, and B. P. Kirtman (1997), A tropical influence on global climate, *J. Atmos. Sci.*, *54*, 1349–1358.

Sellers, W. D. (1969), A climate model based on the energy balance of the Earth-atmosphere system, *J. Appl. Meteorol.*, *8*, 392–400.

M. Cai, Department of Meteorology, Florida State University, Tallahassee, FL 32306, USA. (cai@met.fsu.edu)